

**Please cite the Published Version**

Ghosh, Swarnadipto, Saha, Dipankar, Chakraborty, Ayona, Chakraborty, Samik, Ekpo, Sunday Cookey  and Elias, Fanuel (2023) Design and analysis of mm-Wave MIMO substrate integrated waveguide antenna for multibeam 5G applications. In: 2023 IEEE-APS Topical Conference on Antennas and Propagation in Wireless Communications (APWC), 09 October 2023 - 13 October 2023, Venice, Italy.

**DOI:** <https://doi.org/10.1109/APWC57320.2023.10297489>

**Publisher:** IEEE

**Version:** Accepted Version

**Downloaded from:** <https://e-space.mmu.ac.uk/632135/>

**Usage rights:**  In Copyright

**Additional Information:** © 2023 IEEE. Personal use of this material is permitted. Permission from IEEE must be obtained for all other uses, in any current or future media, including reprinting/republishing this material for advertising or promotional purposes, creating new collective works, for resale or redistribution to servers or lists, or reuse of any copyrighted component of this work in other works.

**Enquiries:**

If you have questions about this document, contact [openresearch@mmu.ac.uk](mailto:openresearch@mmu.ac.uk). Please include the URL of the record in e-space. If you believe that your, or a third party's rights have been compromised through this document please see our Take Down policy (available from <https://www.mmu.ac.uk/library/using-the-library/policies-and-guidelines>)

# Design and Analysis of mm-Wave MIMO SIW Antenna for Multibeam 5G Applications

Swarnadipto Ghosh  
Department of Avionics  
Indian Institute of Space Science &  
Technology  
Thiruvananthapuram, India  
swarnadipto.2000@gmail.com

Dipankar Saha  
Department of Avionics  
Indian Institute of Space Science &  
Technology  
Thiruvananthapuram, India  
dipankarsahauem@gmail.com

Ayona Chakraborty  
Department of Electronics and  
Telecommunication Engineering  
Jadavpur University  
Kolkata, India  
ayonachakraborty1@gmail.com

Samik Chakraborty  
Department of ECE  
Regent Education and Research  
Foundation  
Kolkata, India  
chakrasamik@gmail.com

Sunday Cookey Ekpo  
Department of Engineering  
Manchestar Metropolitan University  
Manchestar, UK.  
s.ekpo@mmu.ac.uk

Fanuel Elias  
Department of Engineering  
Manchestar Metropolitan University  
Manchestar, UK.  
FANUEL.ELIAS@stu.mmu.ac.uk

**Abstract**—This paper presents a slotted substrate integrated waveguide (SIW) multiple input multiple output (MIMO) antenna architecture for mm-Wave/mid-band 5G/6G satellite-cellular applications. An Expo-Gaussian statistical probability density function (PDF) has been introduced as an offset function with rotation to the radiating slots of the proposed MIMO SIW structure. To realize multidirectional multibeam MIMO antenna characteristics, both orthogonal ( $90^\circ$ ) and out-of-phase ( $180^\circ$ ) port switching technique has been established. Equivalent MIMO parameters have been realized through the S-parameters of the proposed MIMO architecture. A closed-form mathematical relationship has been established to characterize the MIMO parameters in the defined frequency band of interest. The proposed PDF rotation function enables the sidelobe level (SLL) and half-power beamwidth (HPBW) to be reduced to  $-20$  dB and  $8.5^\circ$  respectively.

**Keywords**—5G, 6G, antenna, substrate integrated waveguide, MIMO, mm-Wave, satellite-cellular.

## I. INTRODUCTION

Slotted substrate integrated waveguide (SIW) antenna plays a leading role in mm-wave/mid-band 5G/6G satellite-cellular terrestrial on non-terrestrial networks (NTN) communications and different massive MIMO applications [1-5]. mMIMO antennas with highly reduced SLL and directive HPBW are much necessary requirement for different radar scanning and detection technology [6]. By applying different statistical distribution functions on the radiating slot positions [7-9], the required reduced SLL and HPBW can be achieved. In this article, a derived statistical pdf has been incorporated with slot rotations to improve the SLL and HPBW. In later sections, a MIMO architecture has been proposed for multidirectional and multibeam communications.

## II. MATHEMATICAL ANALYSIS OF SIW FOR STATISTICAL DISTRIBUTIONS

In this paper, a mathematically formulated statistical distribution has been modeled to characterize the offset coefficient of the magnetically coupled rectangular slots of the SIW antenna. Along with the statistically distributed rectangular slots, an arithmetically progressed rotation has been applied to the slots. In the further subsections, to establish the concept of offset ( $\Delta g$ ) and rotation ( $\theta$ ) on the magnetically coupled slots of the SIW antenna, Uniform and proposed Expo-Gaussian distribution has been modeled in this paper.

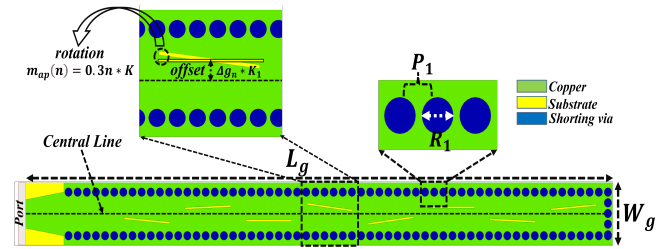


Fig.1. Schematic diagram of the proposed slotted substrate integrated waveguide (SIW) antenna

In Fig.1, the dimensions of the SIW antenna are stated thus:  $L_g=77\text{mm}$ ,  $W_g=7\text{mm}$ ,  $R_1=1\text{mm}$  and  $P_1=1.2\text{mm}$ . The maximum pitch from the center line of the SIW antenna is  $1.5\text{mm}$ . To make an optometric analysis, an offset factor  $m_1=1.5*K_1$  and rotation factor  $m_2=0.3*K$  has been introduced along with the respective statistical distribution co-efficient. A positional symmetry is observed along both the sides of the center line with adjacent  $180^\circ$  phase difference. To modulate the HPBW and SLL level, the respective statistical distribution with the rotation is applied on the magnetically coupled slots of the SIW antenna. On the basis of the controlling basis vector  $K$  and  $K_1$ ; the variation on SLL and HPBW has been mapped into a customized designed  $n^{\text{th}}$  order mathematical equation and realized the behavior through the equivalent contour and residual plots mentioned for different statistical distribution.

### A. Uniform Distribution with Rotation

The probability density function of uniform distribution function can be expressed as

$$f(x) = \begin{cases} 0: x < a \\ \frac{K_1}{b-a}: a < x < b \\ 0: x > b \end{cases} \quad (1)$$

Here,  $K_1$  is defined as the amplitude magnification factor between the maximum pitch range.

Now for the proposed SIW structure, the maximum defined range ( $\frac{1}{b-a}$ ) for the function  $f(x)$  has been mapped with the maximum pitch range. An arithmetically progressed rotation function has been defined for the magnetically coupled slots in (2).

$$m_{ap}(n) = 0.3n * K \quad (2)$$

Here,  $K$  is defined as the magnification factor of rotational function.

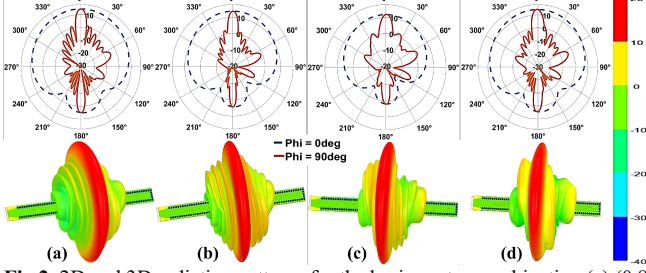


Fig.2. 2D and 3D radiation patterns for the basis vector combination (a) (0.8, 0.1), (b) (0.1, 0.1), (c) (0.2, 0.2), (d) (0.7, 0.3)

According to the proposed design mentioned in Fig.1, vector span of the input basis vectors can be defined as:  $K \in [0.1, 0.8]$  and  $K_1 \in [0.1, 1]$ . For the Uniform distribution function, among the maximum allowable span of the basis vectors, some specified basis combination has been shown for the HPBW and SLL optimization comparison in Fig.2.

From Fig.2 it can be observed that for the basis vector  $(K, K_1) = (0.7, 0.3)$ , the SLL has been reduced by 16.6 dB where the HPBW at  $\phi = 90^\circ$  plane is  $10.15^\circ$  with a peak gain of 14.3 dB at broadside direction. A non-linear customized mathematical relationship has been modelled using cross-correlation between the orthogonally distributed basis vectors to extract the mapping with HPBW and SLL of the proposed SIW antenna for uniformly distributed offset with arithmetically progressed angular rotation. The contour plot (Fig. 3) characterizes the nature of the non-linear relationship between the extracted HPBW and the SLL based on the cross-correlated matrix of  $(K, K_1)$ . From Fig. 3, the efficiency of the regression model is extracted through the Residual plot.

$$HPBW = \sum_{m=0}^N \sum_{n=0}^N P_{mn} x^n y^m \quad (3)$$

The respective co-efficient of the polynomials are mentioned below:

$\begin{matrix} m \\ n \end{matrix}$	0	1	2	3	4
0	9.843	-102.9	1054	-2589	1829
1	35.08	-398.7	859.1	-465.6	0
2	-21.8	213.6	-294.7	0	0
3	0	0	0	0	0

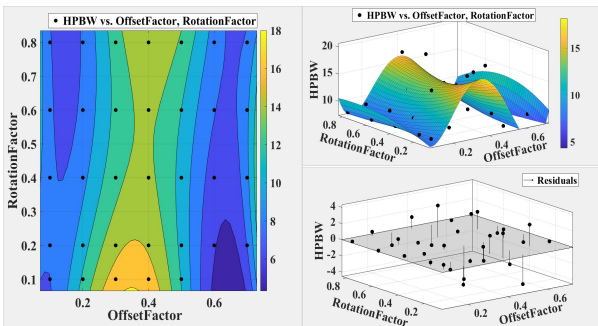


Fig.3. (i) 2D contour plot and (ii) Residual plot between HPBW and co-relation vector matrix of  $K$  &  $K_1$  for uniform distribution with rotation

By observing Table 1, the co-efficient matrix for the HPBW extraction, can be mapped with a sparse matrix where the

higher order co-efficient are diagonally zero. Now, the realization of SLL can be expressed as,

$$SLL = \sum_{m=0}^N \sum_{n=0}^N P_{mn} x^n y^m \quad (4)$$

The respective co-efficient of the polynomials are mentioned below:

$\begin{matrix} m \\ n \end{matrix}$	0	1	2	3	4
0	5.452	109.2	-632.4	1327	-908
1	26.94	-24.41	-97.49	36.17	0
2	-50.72	98.13	69.86	0	0
3	31.33	-90.44	0	0	0

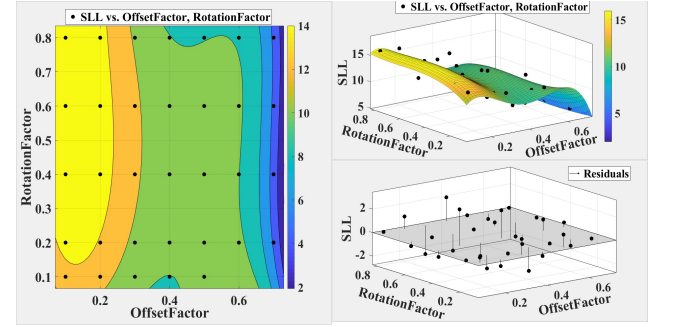


Fig.4. (i) 2D contour plot and (ii) Residual plot between SLL and co-relation vector matrix of  $K$  &  $K_1$  for uniform distribution with rotation

From both the contour plot and the tabular format of the formulated bivariate polynomial expression, the higher-order matrix coefficient returns null to make a sparse matrix.

## B. Expo-Gaussian Distribution with Rotation

An Expo-Gaussian probability density function (PDF) has been proposed in this paper. The function definition for the Expo-Gaussian distribution in (5) can be expressed as:

$$f(x|\sigma, \mu, \lambda) = \frac{1}{\sigma\sqrt{2\pi}} e^{-\frac{(\lambda e^{\lambda|x|} - \mu)^2}{2\sigma^2}} \quad (5)$$

where,  $\sigma$  is the variance,  $\mu$ , the mean,  $\lambda$ , the rate parameter of the defined expo-gaussian PDF in (5).

For the proposed statistical distribution, to make simpler parametric optimization some predefined mathematical assumptions have been taken. In the point of view of Gaussian expression, by taking  $\sigma = 1$  and  $\mu = 0$ , the gaussian distribution is turned into a normal distribution. The independent random variable function  $f(x_1; \lambda) = e^{-\lambda e^{-\lambda|x|}}$  has the rate parameter as  $\lambda$ . To make a simpler optimization, the rate parameter  $(\lambda) = 1$ . Based on this analysis, (5) can be approximated to:

$$f(x|\sigma, \mu, \lambda) = \frac{1}{\sqrt{2\pi}} e^{-\frac{e^{2|x|}}{2}} \quad (6)$$

For the optimum offset locations for the magnetically coupled rectangular slots, the respective coefficients of the specified distributions are  $\Delta g_1 = 0.1994$  mm,  $\Delta g_2 = 0.1990$  mm,  $\Delta g_3 = 0.1961$  mm,  $\Delta g_4 = 0.1760$  mm. To incorporate the arithmetically progressed rotation factor to the slots, the expression in (2) has been applied. For the safe range of operation of the proposed SIW, the offset and rotational angle controlling parameter has a range of  $K \in [0.1, 1.5]$  and  $K_1 \in [0.1, 3.5]$ . The vector basis  $(K, K_1) = (0.6, 0.8)$  (Fig. 5) shows that the SLL has been reduced by 21.97 dB and the HPBW has

been achieved at 7.25 degrees with a peak gain of 17.24 dB in the broadside direction. Customized mathematical models have been designed in (7) and (8) to make a mapping between the orthogonally distributed basis vectors ( $K$  and  $K_1$ ) and the extracted SLL and HPBW for different sets of basis vectors. For a better understanding of the non-linear relationship between the HPBW and the SLL clusters, the vector correlation matrix of offset and rotational angle controlling parameter is represented as contour plots in Figs. 6 and 7 respectively. Table IX shows the respective coefficients of the polynomials.

$$(HPBW)_{Expo-gauss} = \sum_{m=0}^N \sum_{n=0}^N P_{mn} x^n y^m \quad (7)$$

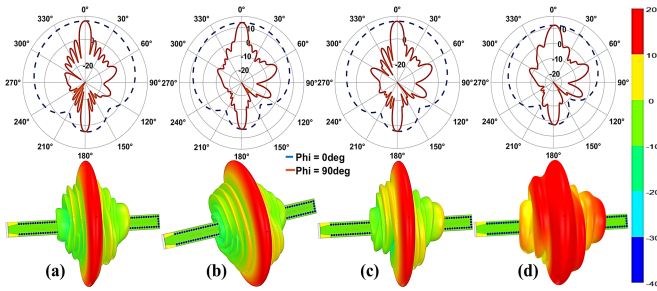


**Fig. 5.** 2D and 3D radiation patterns for the basis vector combination (a) (0.3, 1.15), (b) (0.1, 0.45), (c) (0.6, 0.8), (d) (0.6, 1.5)

TABLE IX  
POLYNOMIAL CO-EFFICIENT FOR  $(HPBW)_{Expo-gaussian}$  MATRIX

$\begin{matrix} m \\ n \end{matrix}$	0	1	2	3	4
0	5.776	2.283	5.444	-4.317	0.6359
1	32.53	-28.05	34.23	-2.631	0
2	-110.6	-32.26	-17.36	0	0
3	184.2	34.46	0	0	0
4	-90.98	0	0	0	0

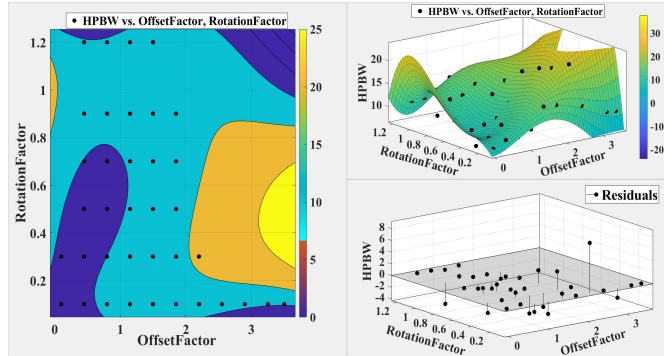


**Fig. 6.** (i) 2D contour plot and (ii) Residual plot between SLL and co-relation vector matrix of  $K$  &  $K_1$  for expo - gaussian distribution with rotation

$$(SLL)_{Expo-gaussian} = \sum_{m=0}^N \sum_{n=0}^N P_{mn} x^n y^m \quad (8)$$

Table X shows the respective coefficients of the polynomials. Since each MIMO system aims for a small weight and power and cost-effective implementation, the key design considerations of the RFFE must improve coverage and efficiency (lowest insertion loss; and excellent power handling); improve capacity (high intermodulation performance); and reduce system size (smallest form factor) [10], [12], [17]-[19].

TABLE X  
POLYNOMIAL CO-EFFICIENT FOR  $(SLL)_{Uniform}$  MATRIX

$\begin{matrix} m \\ n \end{matrix}$	0	1	2	3
0	7.509	17.97	-12.08	2.118
1	4.118	-10.56	2.026	0
2	14.18	-0.7713	0	0
3	-8.396	0	0	0

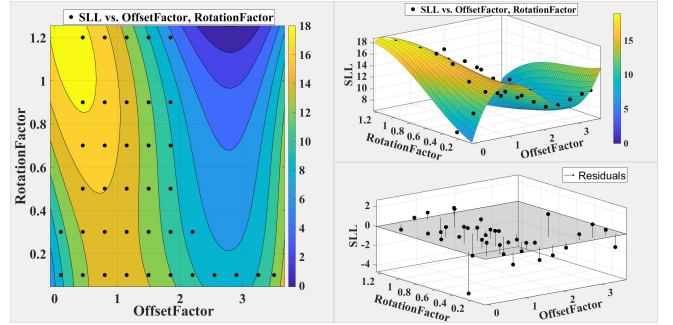


**Fig. 7.** (i) 2D contour plot and (ii) Residual plot between SLL and co-relation vector matrix of  $K$  &  $K_1$  for Expo - Gaussian distribution with rotation

### III. MIMO STRUCTURE OF PROPOSED ANTENNA

In section II, an Expo-Gaussian probability density function was defined to modulate the offset locations of the magnetically coupled rectangular slots. From Fig. 5(c), the HPBW and SLL has been achieved at 7.25° and 17.24 dB respectively for the basis vector combination  $(K, K_1) = (0.6, 0.8)$ . Its narrow beamforming in  $\phi = 90^\circ$  plane can give directive beam-focusing application whereas its fan beam-type radiation pattern at  $\phi = 0^\circ$  plane can give wide scanning applications.

#### A. Rectangular Cube Shaped MIMO Antenna Structure

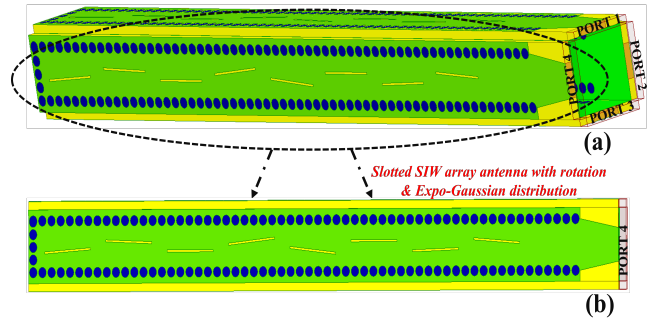


**Fig. 8.** (a) Rectangular Cuboid Shaped MIMO SIW antenna structure (b) Front face cross-section of the proposed MIMO SIW antenna

A rectangular cube shaped MIMO antenna architecture having expo-gaussian distributed and arithmetically progressed slotted SIW array has been proposed in this subsection. Fig. 8 presents the respective rectangular cuboid-shaped MIMO architecture. The radiation patterns (Fig. 5) are the evidence of a wideband beam pattern (nearly  $\theta_{range} = 110^\circ$ ) in three directions from the prismatically arranged MIMO structure. It has been assumed that the MIMO antennas has neither progressive phase shifts ( $\beta$ ) nor any unequal excitation amplitudes in between them. Fig. 9 captures the equivalent S-parameter plots for each excitation port combination of the MIMO system. Fig. 10 shows the 2D polar and 3D radiation pattern.

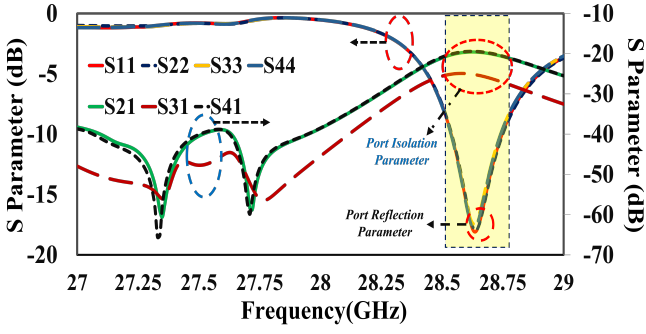


Fig. 9. S-parameters Plots for a MIMO architecture

To modulate multidirectional beam patterns through the prismatically assembled SIW antenna structure, the switching mechanism of the excitation ports can be applied. Using digital switching technique if the excitation ports can be periodically on-off, then the multidirectional beam can be achieved using this MIMO architecture. A detailed analysis is given in below subsection to encounter the multidirectional beam forming by making a digital port switching mechanism.

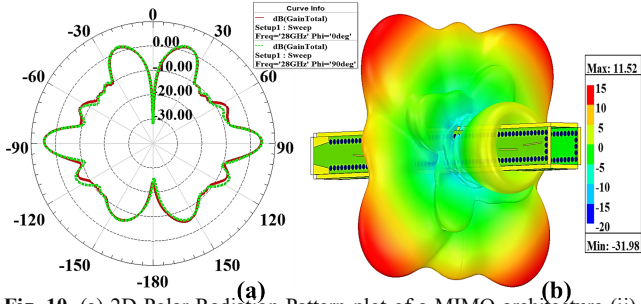


Fig. 10. (a) 2D Polar Radiation Pattern plot of a MIMO architecture (ii) 3D Radiation Pattern

#### IV. MULTIBEAM REALIZATION USING DIGITAL PORT SWITCHING METHOD

Using digital switching method for multiport selection of MIMO systems, multidirectional beamforming can be possible. A periodic digital switching mechanism can enable full beamforming coverage. The different cases for the switching techniques in the proposed SIW MIMO antenna structure are discussed below.

##### A. Orthogonal(90°) Port Switching

In the proposed rectangular cube-shaped MIMO architecture (Fig. 8), among all the possible combinations of ports, the following port combinations can be followed.

$$\{p_1, p_2\} = \{(1,2); (1,4); (2,3); (3,4)\}$$

For all the port combinations, the 3D beam patterns along with the 2D radiation patterns have been captured (Fig. 11).

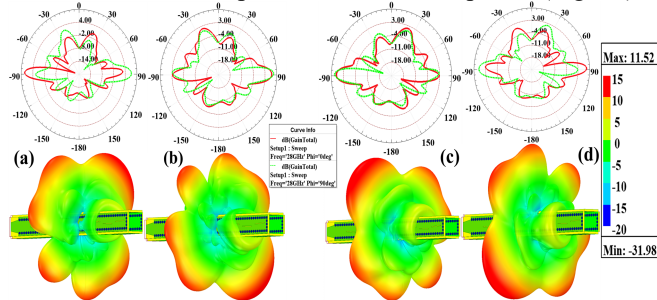


Fig. 11. 2D Polar and 3D Radiation Pattern plot of MIMO architecture for orthogonal port combination of (a){1,2}; (b){1,4}; (c){2,3}; (d){3,4}

##### B. Out-of-Phase (180°) Port Switching

For the proposed rectangular cube-shaped MIMO architecture (Fig. 8), the following combinations of ports have out-of-phase (180°) to each other thus:

$$\{p_1, p_2\} = \{(1,3); (2,4)\}$$

For all the above-mentioned port combinations, Fig. 10 shows the 3D beam patterns along with the 2D radiation patterns.

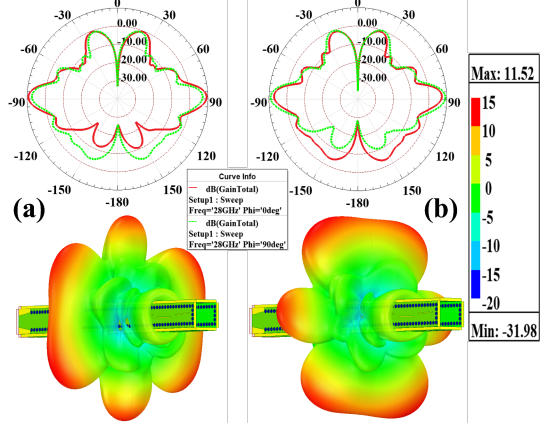


Fig. 12. 2D Polar and 3D Radiation Pattern plot of MIMO architecture for 180° out-of-phase port combination of (a){1,3}; (b){2,4}

#### V. REALIZATION OF MIMO PARAMETERS

To characterize the MIMO antenna system, some MIMO parameters have been analyzed. To synthesize the inner correlation between the excitation ports, envelope correlation co-efficient (ECC) has been analyzed. The effectiveness of the MIMO system has been characterized through diversity gain (DG); total active reflection coefficient (TARC); channel capacity loss (CLL); and mean effective gain (MEG) parameters. The MIMO parameters can be realized through the extracted S-parameters from the MIMO antenna architecture.

$$\rho_e(i, j, M) = \frac{\sum_{m=1}^M S_{mj}^* S_{mi}}{\sqrt{1 - \sum_{m=1}^M |S_{mp}|^2} \sqrt{1 - \sum_{m=1}^M |S_{mq}|^2}} \quad (9)$$

In (10),  $\rho_e(i, j, M)$  is defined as the envelope correlation coefficient for  $(p_i, p_j)$  excitation ports of a M port MIMO architecture. Along with ECC of the proposed MIMO system, the MIMO parameters can be defined as:

$$DG = 10\sqrt{1 - |\rho_e(i, j, M)|^2} \quad (10)$$

$$TARC = \sqrt{\sum_{n=1}^N \frac{|S_{i,n}^* + S_{n,j}|^2}{2}} \quad (11)$$

$$MEG = 0.5 \left[ 1 - \sum_{i=1}^N |S_{ij}|^2 \right] \quad (12)$$

$$CLL = -\log_2 \det(\eta) \quad (13)$$

where;  $\eta$  is defined as  $M \times M$  matrix of channel efficiency factor  $(\sigma_{ij})$  for the Shannon's Channel capacity theorem. The cumulative arrangement of channel efficiency factor  $(\sigma_{ij})$  is  $\eta$  matrix and given by:

$$\eta = \begin{bmatrix} \sigma_{11} & \cdots & \sigma_{1N} \\ \vdots & \ddots & \vdots \\ \sigma_{N1} & \cdots & \sigma_{NN} \end{bmatrix} \quad (14)$$

where the channel efficiency factors  $(\sigma_{ii}$  and  $\sigma_{ij})$  are thus:

$$\sigma_{ii} = 1 - (S_{ii}^2 - S_{ij}^2) \text{ and } \sigma_{ij} = 1 - (S_{ii}^* S_{ij} + S_{ji} S_{jj}^*) \quad (15)$$

For the proposed rectangular cube-shaped MIMO antenna architecture, the MIMO parameters can be characterized for the different switching techniques. To make a sufficient understanding of the MIMO parameters for each defined port combinations, we choose  $\{p_1, p_2\} = (1, 3)$  for  $180^\circ$  out-of-phase switching and  $\{p_1, p_2\} = (1, 2)$  for orthogonal ( $90^\circ$ ) switching. It can be assumed that the correlation effect is independently varied for each switching technique combination. For the proposed rectangular cube-shaped MIMO antenna architecture, we can predict the effect of the MIMO parameters by analyzing the combinations only. The effective port correlation MIMO parameter for both port combinations can be analyzed by replacing the  $(i, j)$  vector combination as per  $180^\circ$  and  $90^\circ$  phase switching for the frequency range of 28.5 GHz– 28.75 GHz. The MIMO parameter variations are captured in Fig. 13.

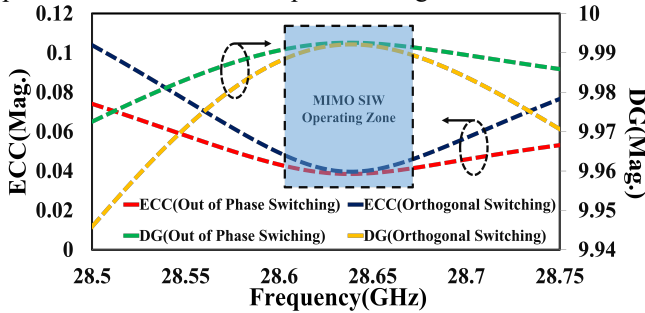


Fig. 13. ECC and DG MIMO parameter for both out of phase and orthogonal switching

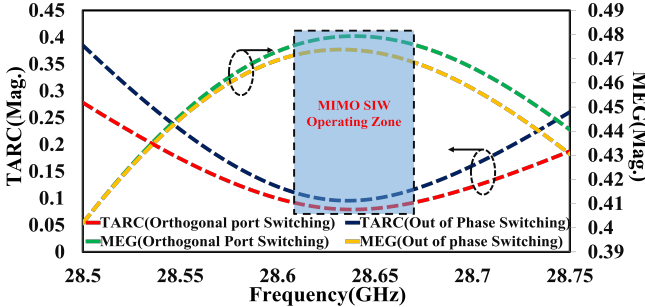


Fig. 14. TARC and MEG MIMO parameter for both out of phase and orthogonal switching

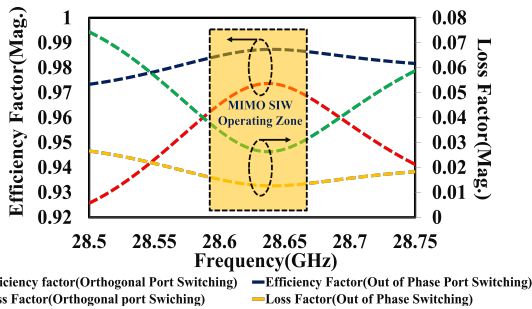


Fig. 15. Efficiency and Loss Factor for both out-of-phase and orthogonal switching of proposed MIMO architecture

Figures 14 and 15 show the respective MIMO parameters. The shaded frequency region (28.60 GHz– 28.65 GHz) are MIMO SIW operating zones due to getting better optimization on port correlation and mean effective gain parameters for both orthogonal and out-of-phase switching techniques. The equivalent channel capacity for the proposed MIMO antenna in (14) is explained in the channel efficiency matrix  $[\eta_{ij}]$ . For

both orthogonal and out-of-phase port switching methods, the equivalent channel efficiency factor ( $\sigma_{ij}$ ) is derived (Fig. 15). A customized mathematical relationship maps the variation of MIMO parameter. This mathematical relationship is helpful for the MIMO characterization of the multibeam SIW antenna operating at the mm-wave band.

## VI. MATHEMATICAL MODELLING OF MIMO PARAMETERS

### A. Modelling of Envelope Correlation Co-efficient (ECC)

For both the orthogonal and out-of-phase port switching techniques, the ECC vs frequency plot is plotted in Fig. 13. The mathematical relationship is obtained thus:

$$ECC_{both} = a_0 + \sum_{n=1}^N a_n \cos(wnx) + b_n \sin(wnx) \quad (16)$$

where  $x$  is the frequency points in between the frequency band. The constant correlation coefficient  $w=12.57$  is defined in (18). Table I shows the respective Fourier coefficients.

TABLE I  
FOURIER COEFFICIENT FOR ORTHOGONAL PORT EXCITATION

$a_0$	$a_1$	$a_2$	$a_3$	$a_4$
0.0754	0.0131	0.0172	0.0004	-0.0023
$b_0$	$b_1$	$b_2$	$b_3$	$b_4$
0	-0.0195	-0.0003	-0.0048	-0.0008

TABLE II  
FOURIER COEFFICIENT FOR OUT OF PHASE PORT EXCITATION

$a_0$	$a_1$	$a_2$	$a_3$	$a_4$
0.0548	0.0109	0.0101	-0.0004	-0.0013
$b_0$	$b_1$	$b_2$	$b_3$	$b_4$
0	-0.0072	-0.0030	-0.0030	-0.0001

### B. Modelling of Diversity Gain (DG)

For both the orthogonal and the out-of-phase port switching techniques, the DG vs frequency is plotted in Fig. 13. The mathematical relationship can be realized thus:

$$DG_{both} = a_0 + \sum_{n=1}^N a_n \cos(wnx) + b_n \sin(wnx) \quad (17)$$

TABLE III  
FOURIER CO-EFFICIENT FOR ORTHOGONAL PORT EXCITATION

$a_0$	$a_1$	$a_2$	$a_3$	$a_4$
9.976	-0.0080	0.0037	0.0014	-0.0007
$b_0$	$b_1$	$b_2$	$b_3$	$b_4$
0	0.0180	0.0041	-0.0025	-0.0004

TABLE IV  
FOURIER COEFFICIENT FOR OUT OF PHASE PORT EXCITATION

$a_0$	$a_1$	$a_2$	$a_3$	$a_4$
9.954	-0.0145	0.0044	0.0023	-0.0007
$b_0$	$b_1$	$b_2$	$b_3$	$b_4$
0	0.03968	0.0066	-0.0024	-0.0006

### C. Modelling of Total Active Reflection Coefficient (TARC)

TABLE V  
GAUSSIAN COEFFICIENT FOR ORTHOGONAL PORT EXCITATION

$a_1$	$a_2$	$a_3$
0.3022	0.2896	0.1254
$b_1$	$b_2$	$b_3$
28.44	28.87	28.54
$c_1$	$c_2$	$c_3$
0.0747	0.1781	0.0794

For both the orthogonal and the out-of-phase port switching methods, the total active reflection coefficient has been analyzed (Fig. 14). A closed-form mathematical relationship has been established to make a non-linear

mapping between TARC and the defined frequency range thus:

$$TARC_{both} = \sum_{n=1}^N a_n e^{\frac{(x-b_n)^2}{c_n^2}} \quad (18)$$

TABLE VI

GAUSSIAN COEFFICIENT FOR OUT OF PHASE EXCITATION

$a_1$	$a_2$	$a_3$
7.524	0.3896	0.1872
$b_1$	$b_2$	$b_3$
28.18	28.85	28.51
$c_1$	$c_2$	$c_3$
0.1662	0.1585	0.0889

#### D. Modelling of Efficiency Factor( $\sigma_{ij}$ )

For both the orthogonal and the out-of-phase port switching techniques, the effective efficiency factor is introduced with respect to a frequency band (Fig. 15). The non-linear mapping mathematical relationship between the efficiency factor ( $\sigma_{ij}$ ) and the given frequency band is thus:

$$E.F_{both} = \sum_{n=1}^N a_n x^n \quad (19)$$

TABLE VII

POLYNOMIAL COEFFICIENT FOR ORTHOGONAL PORT EXCITATION

$a_1$	$a_2$	$a_3$	$a_4$	$a_5$	$a_6$
279.6	-3.98e4	2.275e6	-6.49e7	9.25e8	-5.281e9

TABLE VIII

POLYNOMIAL COEFFICIENT OUT-OF-PHASE EXCITATION

$a_1$	$a_2$	$a_3$	$a_4$	$a_5$	$a_6$
40.1	-5704	3.245e5	-9.228e6	1.312e8	-7.464e8

#### E. Modelling of Loss Factor

For both the orthogonal and the out-of-phase ports excitations, the mutual loss factor has been modeled with respect to the frequency band (Fig. 15). We have derived a closed-form mathematical relationship to achieve a non-linear mapping between the loss factor and the frequency thus:

$$L.F_{both} = a_0 + \sum_{n=1}^N a_n \cos(wnx) + b_n \sin(wnx) \quad (20)$$

Other statistical PDFs can be modeled for better SLL and HPBW optimization and reconfigurable MIMO RF frontend architecture [10]-[14] for multidirectional and multibeam satellite-cellular 5G/6G communications [15]-[19].

TABLE IX

FOURIER CO-EFFICIENT FOR ORTHOGONAL PORT EXCITATION

$a_0$	$a_1$	$a_2$	$a_3$	$a_4$
0.0486	0.0063	0.0203	0.0014	-0.00243
$b_0$	$b_1$	$b_2$	$b_3$	$b_4$
0	-0.0037	0.00306	-0.00516	-0.00103

TABLE X

FOURIER COEFFICIENT FOR OUT-OF-PHASE PORT EXCITATION

$a_0$	$a_1$	$a_2$	$a_3$	$a_4$
0.01717	0.00397	0.00603	0.00018	-0.0007
$b_0$	$b_1$	$b_2$	$b_3$	$b_4$
0	0.001016	-8.07e-5	-0.00162	-0.000019

## VII. CONCLUSION

The effect of statistically modeled probability density function with rotation as an offset function of the proposed substrate integrated waveguide antenna on the reduction of sidelobe level and half-power bandwidth is effective than the uniform distribution. The mathematical modeling of MIMO antenna parameters achieved the HPBW and SLL at 7.25°

and 17.24 dB respectively. The equivalent MIMO architecture gives the multidirectional multibeam response by realizing the orthogonal (90°) and out-of-phase (180°) port switching techniques for the proposed SIW antenna for 5G/6G networks.

## REFERENCES

- [1] Bozzi, Maurizio, Anthimos Georgiadis, and Kaijie Wu. "Review of substrate-integrated waveguide circuits and antennas." *IET Microwaves, Antennas & Propagation* 5, no. 8 (2011): 909-920.
- [2] Deslandes, Dominic, and Ke Wu. "Design consideration and performance analysis of substrate integrated waveguide components." In *2002 32nd European microwave conference*, pp. 1-4. IEEE, 2002.
- [3] Luo, Guo Qing, Zhi Fang Hu, Lin Xi Dong, and Ling Ling Sun. "Planar slot antenna backed by substrate integrated waveguide cavity." *IEEE Antennas and Wireless Propagation Letters* 7 (2008): 236-239.
- [4] Trinh-Van, Son, Jong Min Lee, Youngoo Yang, Kang-Yoon Lee, and Keum Cheol Hwang. "A Sidelobe-Reduced, Four-Beam Array Antenna Fed by a Modified 4×4 Butler Matrix for 5G Applications." *IEEE Transactions on Antennas and Propagation* 67, no. 7 (2019): 4528-4536.
- [5] Ali, Mohd Tarmizi, Tharek Bin Abdul Rahman, Muhammad Ramlie Kamarudin, Mohd Nor Md Tan, and Ronan Sauleau. "A planar antenna array with separated feed line for higher gain and sidelobe reduction." *Progress in electromagnetics Research*, vol. 8 pp. 69-82, 2009.
- [6] Goto, Naohisa, and D. Cheng. "Sidelobe-reduction techniques for phased arrays using digital phase shifters." *IEEE Transactions on Antennas and Propagation*, vol. 18, no. 6, pp. 769-773, 1970.
- [7] Chen, Xiao-Ping, and Ke Wu. "Substrate integrated waveguide filter: Basic design rules and fundamental structure features." *IEEE Microwave Magazine*, vol. 15, no. 5, pp. 108-116, 2014.
- [8] Li, Teng, and Wen Bin Dou. "Millimetre-wave slotted array antenna based on double-layer substrate integrated waveguide." *IET Microwaves, Antennas & Propagation*, vol. 9, no. 9, pp. 882-888, 2015.
- [9] D. Saha, C. Saha and J. Y. Siddiqui, "Binomially Distributed Slotted Array Antenna with Highly Reduced Sidelobe Level," *2022 IEEE 19th India Council International Conference (INDICON)*, Kochi, India, 2022, pp. 1-3, doi: 10.1109/INDICON56171.2022.10039877.
- [10] I. Lau, S. C. Ekpo, M. Zafar, M. Ijaz, and A. Gibson, "Hybrid mmWave-Li-Fi 5G Architecture for Reconfigurable Variable Latency and Data Rate Communications," in *IEEE Access*, vol. 11, pp. 42850-42861, May 2023; https://doi.org/10.1109/ACCESS.2023.3270777.
- [11] S. Ekpo and D. George, "Impact of Noise Figure on a Satellite Link Performance," *IEEE Communications Letters*, Vol. 15, No. 9, pp. 977-979, June 2011; https://doi.org/10.1109/LCOMM.2011.072011.111073.
- [12] S. Ekpo, B. Adebisi, and A. Wells, "Regulated-element Frost Beamformer for Vehicular Multimedia Sound Enhancement and Noise Reduction Applications," in *IEEE Access J.*, vol. 5, pp. 27254-27262, Dec. 2017; https://doi.org/10.1109/ACCESS.2017.2775707.
- [13] M. Zafar, S. Ekpo, J. George, P. Sheedy, M. Uko and A. Gibson, "Hybrid Power Divider and Combiner for Passive RFID Tag Wireless Energy Harvesting," in *IEEE Access*, vol. 10, pp. 502-515, Dec. 2022, DOI: https://doi.org/10.1109/ACCESS.2021.3138070.
- [14] S. Ekpo, and D. George, "4-8 GHz LNA design for an adaptive small Satellite Transponder using InGaAs PHEMT Technology," in *Proc. 11th IEEE Wireless & Microwave Conference*, Melbourne FL, USA, April 2010, pp. 1-4; https://doi.org/10.1109/WAMICON.2010.5461877.
- [15] S. C. Ekpo, "Parametric System Engineering Analysis of Capability-based Small Satellite Missions," *IEEE Systems Journal*, Vol. 13, No. 3, pp. 3546-3555, September 2019; https://doi.org/10.1109/JSYST.2019.2919526.
- [16] S. C. Ekpo, "Thermal Subsystem Operational Times Analysis for Ubiquitous Small Satellites Relay in LEO," in *International Review of Aerospace Engineering J.*, Vol. 11, No. 2, pp. 48-57, Apr. 2018. DOI: https://doi.org/10.15866/irease.v11i2.13663.
- [17] M. Uko, and S. Ekpo, "8-12 GHz pHEMT MMIC Low-Noise Amplifier for 5G and Fiber-Integrated Satellite Applications," in *Int'l Review of Aerospace Engineering J.*, Vol. 13, No. 3, pp. 99-107, Jun. 2020. DOI: https://doi.org/10.15866/irease.v13i3.17998.
- [18] Olugbenga Sowande, Francis Idachaba, Sunday Ekpo, Nasir Faruk, Mfonobong Uko, Olugbenga Ogunmodimu, "Sub-6 GHz 5G Spectrum for Satellite-Cellular Convergence Broadband Internet Access in Nigeria," *Int'l Review of Aerospace Eng. J.*, Vol. 15, No. 2, pp. 85 - 96; https://doi.org/10.15866/irease.v15i2.20240.
- [19] S. Ekpo and D. George, "A System Engineering analysis of highly adaptive small Satellites," *IEEE Systems Journal*, Vol. 7, No. 4, pp. 642-648, Sep. 2013; https://doi.org/10.1109/JSYST.2012.2198138.